Asian Journal of Chemistry; Vol. 35, No. 8 (2023), 1891-1898

ASIAN JOURNAL OF CHEMISTRY

https://doi.org/10.14233/ajchem.2023.28049

Structural and Multiple Applicational Studies of Alkaline Earth Metal Spinel (AB_2O_4) Ferrites

S. SWAMY[1], D.B. ARUNA KUMAR[1,*], K. GURUSHANTHA[2], S. MEENA[3,*], K. KESHAVAMURTHY[4] and N. BASAVARAJU[5]

[1]Department of Studies and Research in Chemistry, University College of Science, Tumkur University, Tumkur-572103, India
[2]Department of Chemistry, M.S. Ramaiah Institute of Technology (Affiliated to Visvesvaraya Technological University, Belgaum), Bengaluru-560054, India
[3]Department of Chemistry, Dayananda Sagar College of Engineering, Bengaluru-560078, India
[4]Department of Physics, Dayananda Sagar College of Engineering, Bengaluru-560078, India
[5]Department of Physics, East West Institute of Technology, Bengaluru-560091, India

*Corresponding authors: E-mail: nirmaldb@gmail.com; meena23286@gmail.com

Received: 27 May 2023; *Accepted*: 27 June 2023; *Published online*: 31 July 2023; AJC-21322

The spinel ferrites MFe_2O_4 from alkaline earth metals (M = Mg, Ca, Sr, Ba) were identified as potential photocatalyst. The present work deals with the synthesis of mentioned ferrites by solution combustion synthesis using urea as fuel. X-ray pattern displays the formation of pure phase, whereas the functional groups were confirmed by FTIR studies. The UV-DRS spectra revealed that $MgFe_2O_4$ (2.3 eV) had an energy band gap that was optimal for visible light phototcatalytic degradation. The ferrites $MgFe_2O_4$, $CaFe_2O_4$, $SrFe_2O_4$ and $BaFe_2O_4$ displays excellent photocatalytic degradation performance for reactive blue 4 dye under visible light within 120 min resulted 93%, 84%, 92% and 79%, respectively. Compared to other synthesized ferrites $SrFe_2O_4$ shows remarkable specific capacitance with 288.7×10^{-3} F/g ascertains the super capacitor nature and also indicates better results to sense lead nitrate at very lower concentrations from cyclic voltammogram studies. The antibacterial activity against *Bacillus* and *Pseudomonas* (30 mg/mL) showed that $CaFe_2O_4$ was more effective than other synthesized ferrites.

Keywords: Spinel ferrites, Alkaline earth metals, Urea, Photocatalyst, Reactive blue 4 dye, Antibacterial activity.

INTRODUCTION

In relation to energy and environment, there seems to be a rapid expansion in the field of nanotechnology for the past four decades to identify an efficient material in the field of heterogeneous photocatalysis [1-3]. There seems to be synthesis of many efficient nanomaterials for its successful application towards photocatalysis, supercapacitor, as a sensor and for antibacterial activity. There is also a significant increase in multidisciplinary nature of the synthesized nanomaterials nowadays. The efficiency of the synthesized materials is associated to its advances in the field of nanotechnology field as it allows a control of size and morphology [4,5]. There was a complete lack of order in the reporting of synthetic ferrites made from alkaline earth metals [6,7]. This drives the pursuit of more reliable and powerful catalysts that can be energized by sunshine.

Considering this view, in modern technology, ferrites with AB_2O_4 unit (B = Fe^{3+} and A = M^{2+}) are complex oxides exhibits interesting physical and chemical properties with promising applications in photocatalysis [8], gas sensing [9], *in vitro* cytotoxicity [10], diagnosis as well as treatment related to magnetic devices [11], high density data storage and magnetic carriers for site-specific drugs delivery [12]. Nanosized ferrites plays an essential role in photocatalysis due to their large surfaces that enhances the absorption along with the sensor response. All the alkaline earth metal ferrites possess an energy band gap of around 2 eV or less than that and well absorb huge amount of solar light leading to enriched photocatalytic activity [13]. Unlike other wideband gap semiconductor, ferrites easily accept the visible light and remove the contaminants from water, air and can support for bacterial inactivation.

$MgFe_2O_4$ is one of the promising photocatalyst because of its stability, limited band gap and low sensitivity to photoanodic corrosion [14,15], whereas $CaFe_2O_4$ exhibits superlative performance, more biocompatible as calcium is non-toxic in nature. Similarly, $SrFe_2O_4$ has great potential for the photo-

decomposition along with hydrogen production [16-18]. It can be prepared at very high temperature and also possess optical properties with low band gap energy within the visible spectrum [19]. $BaFe_2O_4$ was chosen due to its less cost, curie temperature of high level, excellent chemical stability and high saturation magnetization [20-23].

Even though many researchers imply the importance of these ferrites as photocatalyst, it need to be explored towards other applications. Thus, due to the huge importance of ferrite materials in environmental applications, supercapacitors and sensors, herein, a sincere effort has been undertaken to synthesize alkaline earth metal ferrites. In this work, the possible uses of the alkaline earth metal ferrite, including its properties as a supercapacitor and its ability to detect extremely low concentrations of lead nitrate, which has antibacterial properties are discussed. The nanoferrites from from alkaline earth metals (M = Mg, Ca, Sr, Ba) were prepared *via* solution combustion synthesis using the biofuel urea and analyzed for various characterization such as PXRD, FTIR, SEM and UV-DRS techniques.

EXPERIMENTAL

All the analytical grade chemicals *viz*. magnesium nitrate hexahydrate [$Mg(NO_3)_2{\cdot}6H_2O$], calcium nitrate tetrahydrate [$Ca(NO_3)_2{\cdot}4H_2O$], strontium nitrate [$Sr(NO_3)_2$], barium nitrate [$Ba(NO_3)_2$], iron nitrate nonahydrate [$Fe(NO_3)_2{\cdot}9H_2O$], urea and reactive blue 4 were procured from S.D. Fine Chemicals and used as such.

Synthesis: For the synthesis of magnesium ferrite, 1:2 ratio of magnesium nitrate hexahydrate and iron nitrate nonahydrate were taken in a cylindrical petri dish. Required amount of urea (oxidized fuel ratio was 1) added to petridish containing iron nitrate and magnesium nitrate, 50 mL of distilled water was transferred to dissolve and make homogenous solution by using magnetic stirrer. The mixture was mixed well with magnetic stirrer for 20 min at 60 ºC to get viscous solution. The petridish containing homogeneous viscous redox mixture solution was kept inside a preheated muffle furnace at 450 ± 5 ºC. The solution started to boils then dehydration occurs. The solution starts decomposes resulted to the formation of magnesium ferrites with large amount of gasses liberated. The entire process was completed within 10 min. The obtained magnesium ferrite was calcinated at 600 ºC for 3 h. Similarly, the other alkaline metal ferrites *viz*. calcium, strontium and barium ferrites were also prepared.

Charactization: The crystallinity nature of the obtained final products were characterized employing Bruker PXRD, whereas the morphological characteristics and the size of the particle was investigated by scanning electron microscopy (SEM, Hitachi-3000). The UV-visible reflectance spectra was measured on Perkin-Elmer UV-visible Lambda 365 spectrophotometer. FTIR spectra was taken in a Perkin-Elmer FTIR spectrometer (Spectrum-1000). An electrochemical analyser CHI608E potentiostat with a trielectrode system was used to measure the cyclic voltammetry (CV), EIS and sensor measurements which includes combined graphite powder electrode, platinum wire and Ag/AgCl as working, counter and reference electrodes, respectively and 1.0 M KCl solution as electrolyte.

Antibacterial activity: Antibacterial assay of the alkaline metal ferrites (M = Mg, Ca, Ba and Sr) was measured as zone of inhibition on agar well diffusion plate. Briefly, 30 mg/mL concentration of prepared alkaline earth metal ferrites were prepared in deionized water and loaded into well created on solidified Muller Hinton Agar (MHA) plates seeded with 50 µL of test organism *Bacillus* and *Pseudomonas*. Ampicillin was used as a positive control. The plates were allowed to incubate at 37 ºC and recorded for zone of inhibition after 24 h.

Photocatalytic degradation studies: Photocatalytic activity of prepared alkaline earth metal ferrites was evaluated by taking reactive blue 4 as a reference dye, which is available commercially. A stock solution of reactive blue 4 dye (1000 ppm) was prepared by using distilled water. Then, 250 mL of 10 ppm of reactive blue 4 dye solution was prepared from the stock solution and transferred into circular glass reactor having the surface area 176 cm^2. Optimized 0.07 g of alkaline ferrite (Mg, Ca, Sr and Ba) catalyst was transferred into circular glass reactor containing reactive blue 4 solutions and stir the solution in dark condition for 30 min by using magnetic stirrer to check the adsorption and desorption equilibrium of dye and catalyst. Visible light was allowed on reactive blue 4 solution containing catalyst in an open air. A 4 mL of reaction mixture were collected at regular time interval of 15 min and centrifuged to remove the catalyst and subjected for degradation of reactive blue 4 was determined using UV-Visible spectrophotometer. The percentage of reactive blue 4 dye degradation (D_g) with respect to time was estimated using eqn. 2:

$$D_g = \frac{C - C_a}{C} \times 100 \quad (2)$$

RESULTS AND DISCUSSION

Powederd XRD studies: Fig. 1 represents the PXRD pattern of the prepared alkaline earth metal ferrites. All the synthesized nanomaterials show pure phase without any impurity. In case of $MgFe_2O_4$, the plane at (311) corresponds to the spinel ferrite formation. All the observed diffraction peaks confirm the presence of centroid cubic structure of ferrites with JCPDS

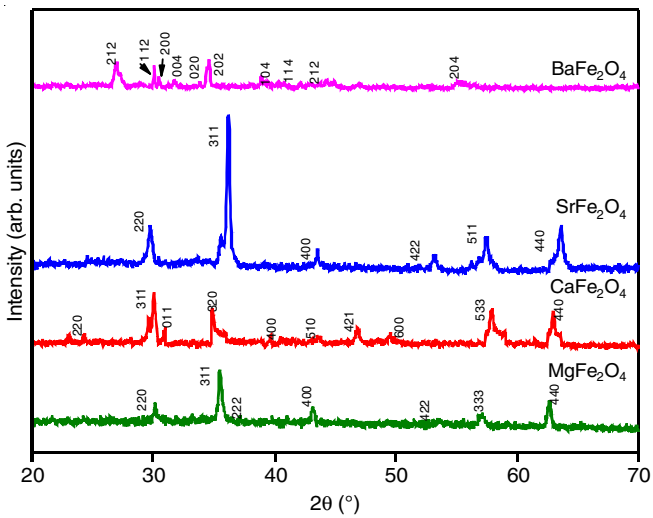

Fig. 1. PXRD spectra of synthesized alkaline earth metal ferrites

card No. # 88-193536-0398 [24]. All the indexed peaks of $CaFe_2O_4$ matched well with JCPDS card no. #78-4321 indicating the formation of orthorhombic structure with good purity [25]. The $SrFe_2O_4$ spectra indicates the nanocrystalline nature of typical peak of spinel ferrite with cubic structure [JCPDS card no. #0001-2027] [26,27]. The XRD data of $BaFe_2O_4$ exhibited the orthorhombic structure and are well-matched as per JCPDS card no. 46-0113 [28].

SEM studies: Fig. 2 represents the surface morphology of the prepared alkaline earth metal ferrites along with the

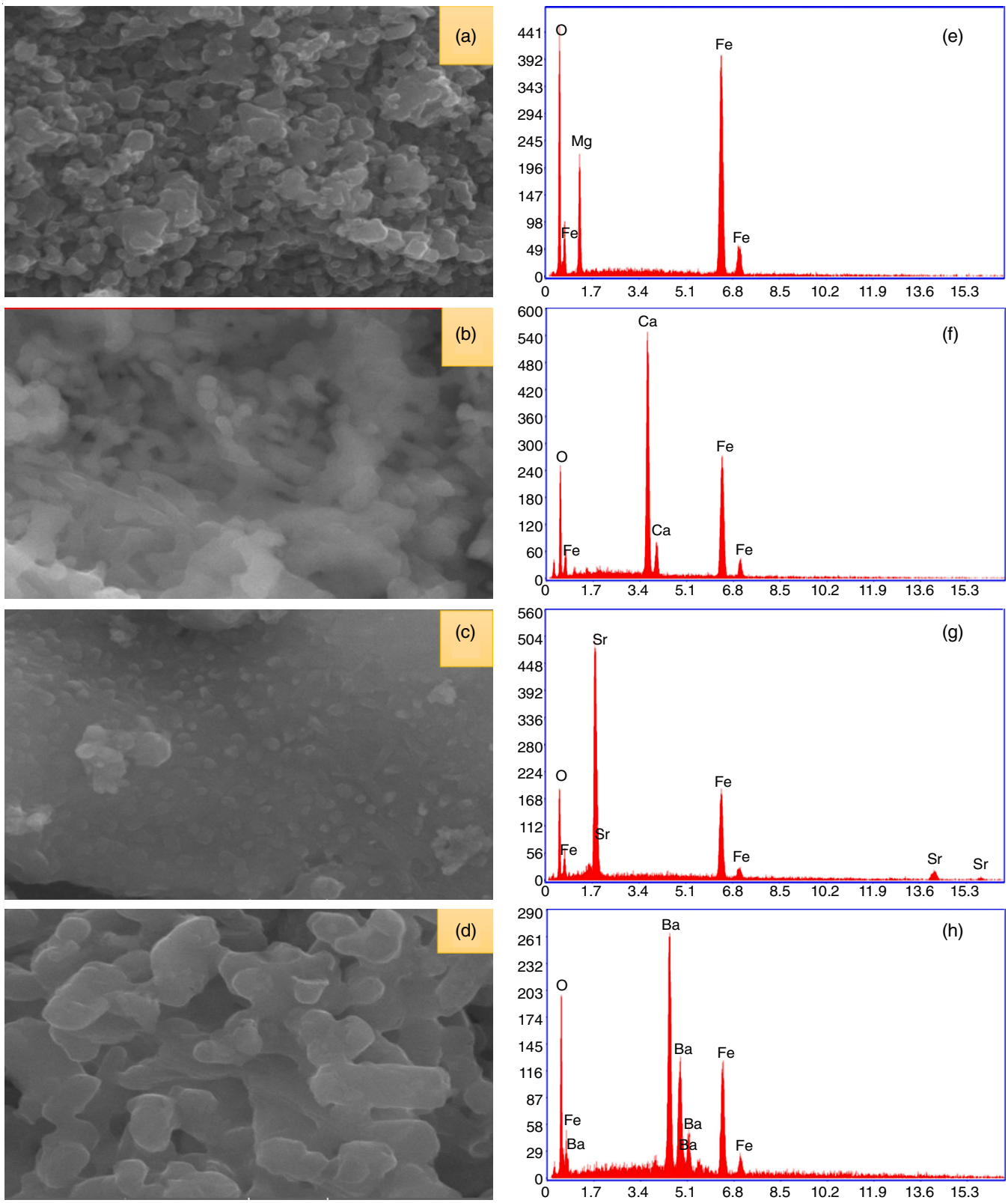

Fig. 2. SEM and EDAX images of (a & e) $MgFe_2O_4$ (b & f) $CaFe_2O_4$ (c & g) $SrFe_2O_4$ (d & h) $BaFe_2O_4$, respectively

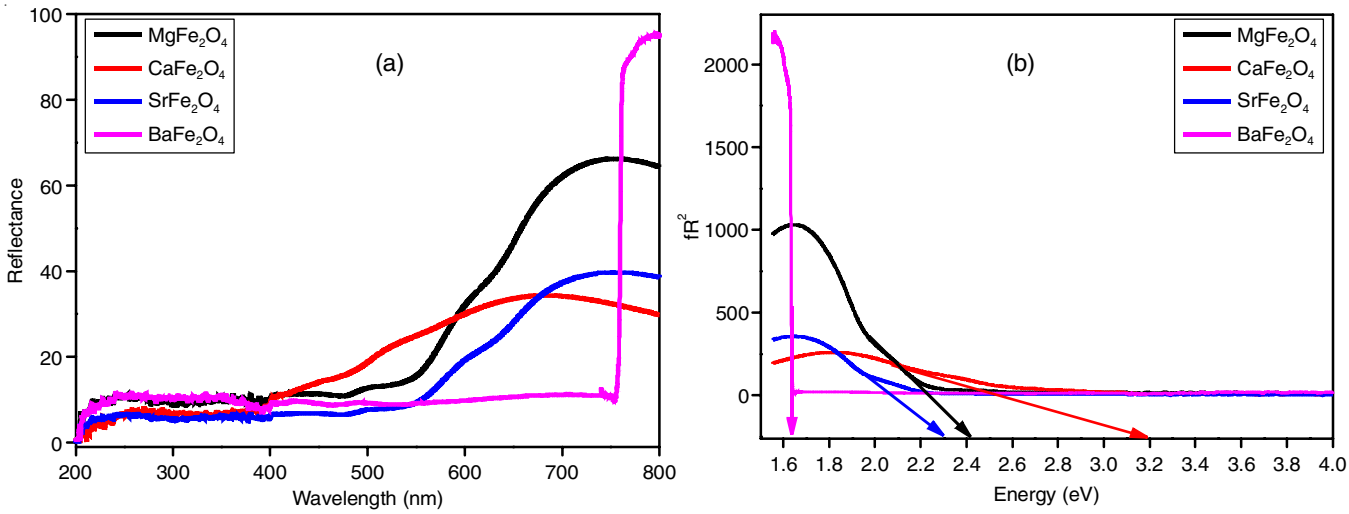

Fig. 3. Reflectance spectra (a) and their band gap graph (b) of alkaline earth metal ferrites

EDAX. $MgFe_2O_4$ possess very small particles with agglomeration (Fig. 2a), whereas $CaFe_2O_4$ have fine grain structure with pores and voids (Fig. 2b). The structure of $SrFe_2O_4$ was found to be soft and smooth surface nature with slight grains appearance (Fig. 2c), moreover the $BaFe_2O_4$ shows larges grains with agglomerations and voids (Fig. 2d).

Diffused reflectance spectral (DRS) analysis: The DRS analysis of the prepared ferrites are depicted in Fig. 3. The strong absorption bands of alkaline earth metal ferrites were observed in the range from 400 to 800 nm and few narrow absorption peaks in the wavelength of 230 to 400 nm was also observed. The energy band gap (E_g) of the prepared ferrites were calculated by plotting energy (hν) *vs.* $F(R)^2h\nu$ as elucidated from Kubelka-Munk equation (eqn. 1):

$$F(R) = \frac{(1-R)^n}{2R} = \frac{K}{S} \quad (1)$$

The obtained energy band gap of synthesized $MgFe_2O_4$, $CaFe_2O_4$, $SrFe_2O_4$, $BaFe_2O_4$ nanoferrites were found to be 2.3, 2.8, 2.4 and 1.65 eV, respectively as depicted in Fig. 3b. Thus, the $MgFe_2O_4$ verified a relatively narrow band gap of 2.3 eV, indicating that the higher photo-response in the visible light compared to other prepared ferrites.

FTIR studies: Fig. 4 shows the FTIR spectra of the prepared ferrites, where a wide band around 3354 cm^{-1} was ascribed to the stretching and bending vibrations of O–H bond. The OH peaks were associated to the water molecules absorbed over the surface of the ferrites. The peaks around at 880 cm^{-1} was assigned to the stretching vibrations of M-O-M (M = Fe/Ba/Mg/Sr/Ca). The bands near the range of 600-500 cm^{-1} and 470-450 cm^{-1} are belongs to tetrahedral and octahedral sites, respectively which ascertains the availability of oxygen-metal tensile bonds in spinel ferrite [29].

Antibacterial activity: According to the well-diffusion screening of alkaline ferrites were clearly possess antibacterial properties against *Bacillus* and *Pseudomonas*. Among four alkaline ferrites, calcium ferrites has showed appreciable zone of inhibition 0.77 ± 0.03 mm and 0.27 ± 0.03 mm, respectively for *Bacillus* and *Pseudomonas* (Fig. 5). Among the prepared

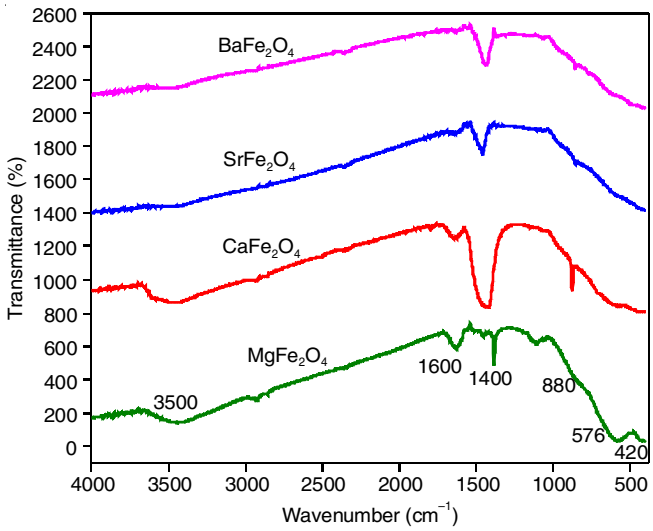

Fig. 4. FTIR spectra of alkaline earth metal ferrites

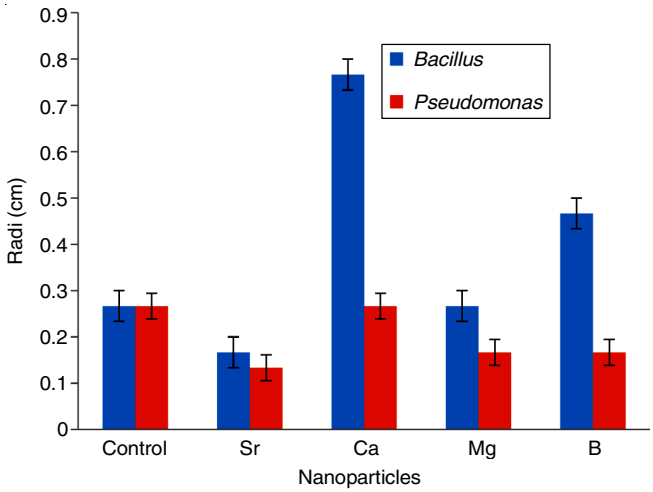

Fig. 5. Antibacterial activity of alkaline earth metal ferrites

alkaline ferrites, strontium ferrites had the smallest growth inhibition zone. The Gram-positive bacteria were more liable, which may be due to the difference in the cell wall composition.

Photocatalytic degradation studies: The absorbance spectra of reactive blue 4 dye degradation with interval of time 15 min using prepared alkaline earth metal ferrites is shown in Fig. 6a-d. It clearly shows that the maximum peak intensity at 485 nm decreases with increase in time interval hence, it confirms that reactive blue 4 degraded. The percentage degradation of reactive blue 4 using $MgFe_2O_4$, $CaFe_2O_4$, $SrFe_2O_4$ and $BaFe_2O_4$ as catalyst was found to be 93%, 84%, 86% and 89 % respectively (Fig. 6f and Table-1).

TABLE-1
KINETIC STUDIES UNDER UV LIGHT ON ALKALINE EARTH METAL FERRITES PHOTOCATALYSTS

Photocatalysts	Degradation (%)	$k \times 10^{-3}$ (min^{-1})
$MgFe_2O_4$	93	29.04
$CaFe_2O_4$	84	24.94
$SrFe_2O_4$	92	19.30
$BaFe_2O_4$	79	20.81

Mechanism: The catalyst alkaline ferrite in reactive blue 4 dye solution generates electron hole pairs when visible light falls on it due to absorption of light. The generated electrons in conduction band react with dissolved oxygen in dye solution to form super oxide anion (O_2^-), in addition to that H_2O reacts with holes in the valence band to form $^{\bullet}OH$ radicals. The generated superoxide anions (O_2^-) and $^{\bullet}OH$ radicals reacts with reactive blue 4 molecules and degradation occurs. Magnesium ferrites shows the highest degradation of reactive blue 4 may be due to optimum energy band gap of 2.3 eV.

Reusebility: The recyclability of photocatalyst is more essential for practical approaches. To understand the recyclability of the prepared alkaline earth metal ferrites, 5 consecutive cyclic dye degradation experiments were carried out using the ferrite catalyst. After each cycle, the catalyst can be removed using the external magnet and washed dried for the next cycle. The cyclic runs of dye degradation is shown in Fig. 6e, the results proven that prepared ferrite photocatalyst retains after 5 consecutive runs of experiments with meager reduction in the degradation percentage confirms that the prepared alkaline earth metal ferrites is suitable for the industrial applications.

Electrochemical studies: The electrochemical analysis were performed in combination of three-electrode with 1.0 M KCl as the aqueous electrolyte at room temperature. Analysis includes cyclic voltammetry (CV), electrochemical impedance (EIS) and sensor studies were experimented. The specific capacitance (Scp) can be evaluated for the synthesized electrode from CV by eqn. 3:

$$Scp = \frac{\int IdV}{\nu \times m \times \Delta V} \quad (3)$$

where I = current, V = potential, m = electrode mass, ν = scan rate and ΔV = operating voltage window.

The electrochemical performance of $MgFe_2O_4$, $CaFe_2O_4$, $SrFe_2O_4$ and $BaFe_2O_4$ was assessed through cyclic voltammetry (CV) by the three-electrode system. The curves from CV of $MgFe_2O_4$, $CaFe_2O_4$, $SrFe_2O_4$ and $BaFe_2O_4$ at various scan rate are shown in Fig. 7a-d, which confirms the ideal capacitive behaviour having rectangular shape of cyclic voltammogram (CV). The curve validated that CV curves progressively shifted and sloped along with the increase of scan rate by retaining the shape, it is maintaining the rectangular position and electrochemical stability even when scan rate increases. Among the prepared alkaline metal ferrite, $SrFe_2O_4$ displayed a higher space area below the CV curve signifying higher value of Scp of 288 × 10^{-3} F/g than other ferrites. The Scp value of all the

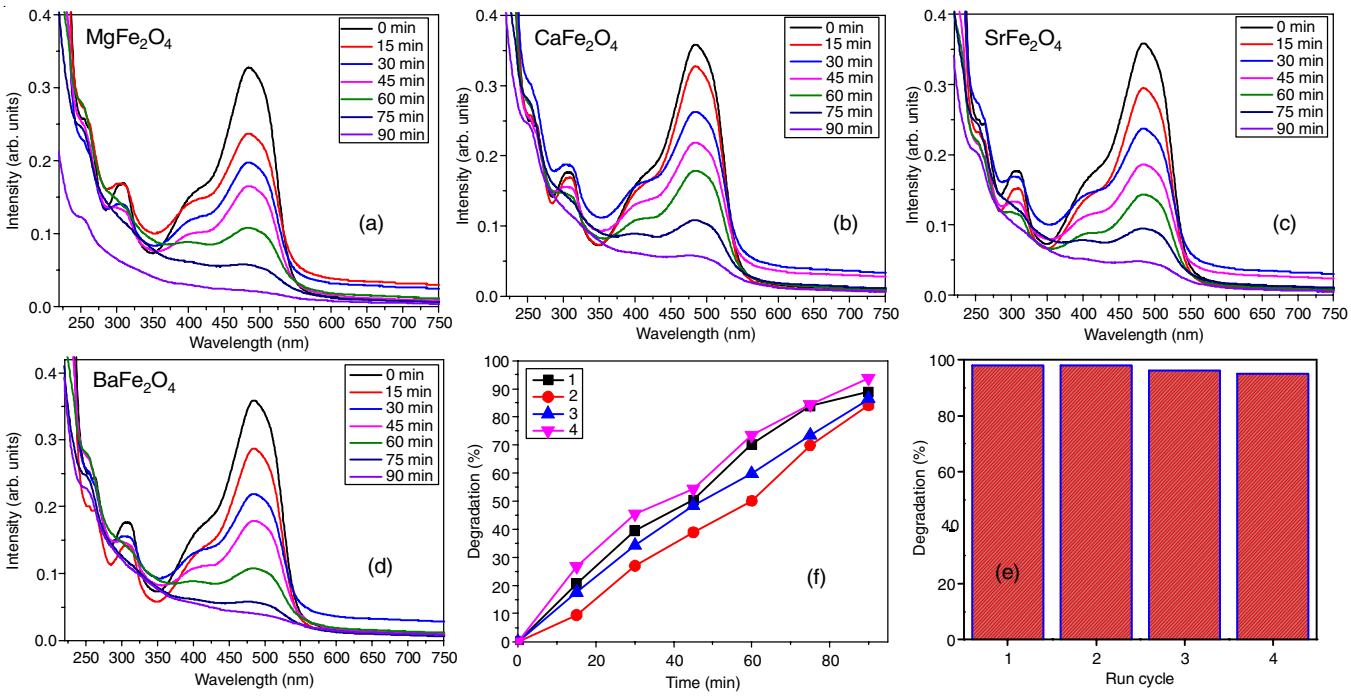

Fig. 6. (a-d) Absorbance graph for the dye degradation by alkaline earth metal ferrites, (f) % degradation of dye, (e) recyclic graph of alkaline earth metal ferrites for dye degradation

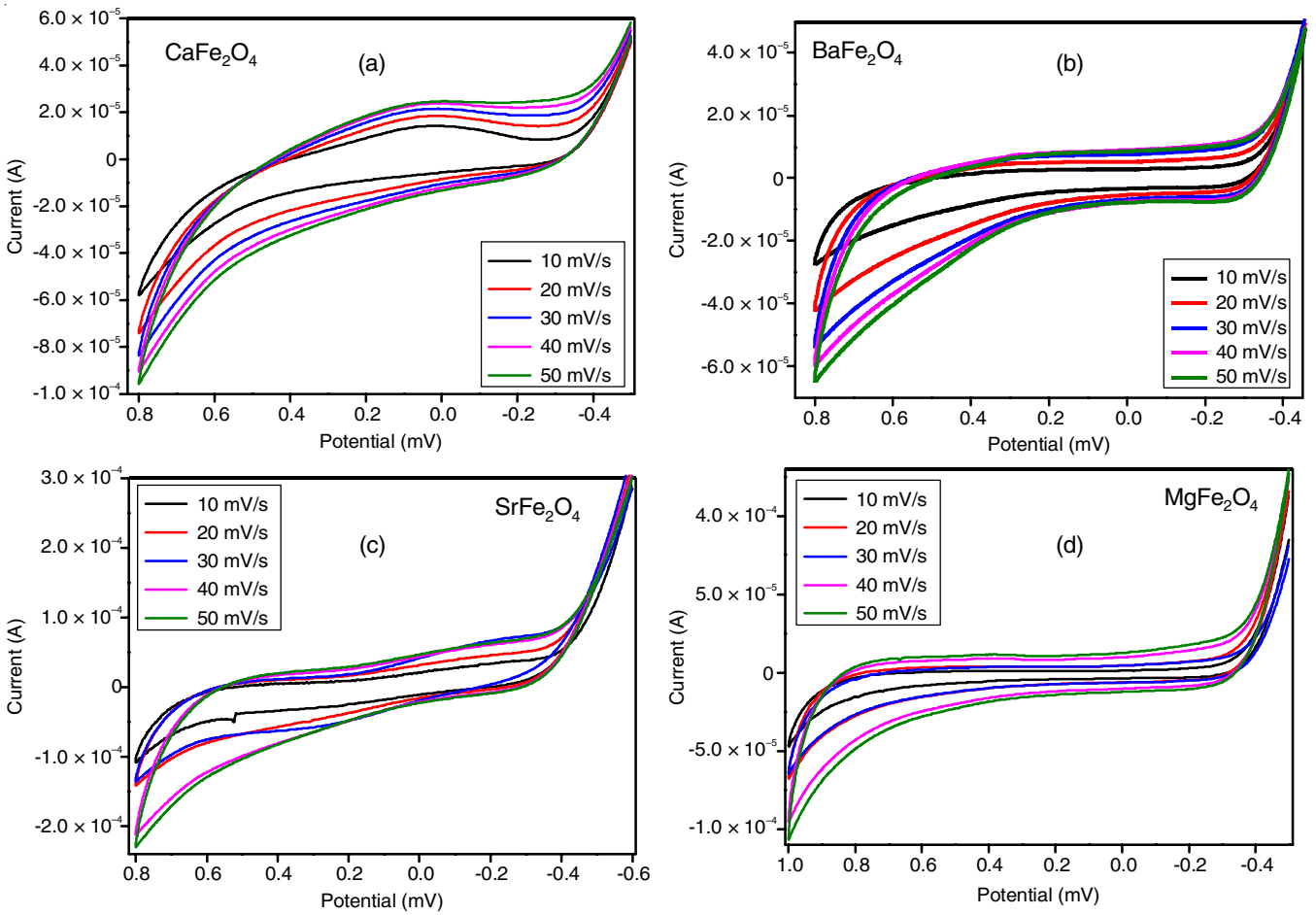

Fig. 7. CV graph of synthesized alkaline earth metal ferrites at various scan rates

prepared ferrite electrode at 0.01, 0.02, 0.03, 0.04 and 0.05 V/s scan rates are given in Table-2. The Scp values decreased as the scan rate increases due to the slower penetration of the electrolytic ions into the pores of the sample at higher scan rate [29,30].

TABLE-2
SPECIFIC CAPACITANCE DATA FROM CV OF SYNTHESIZED ALKALINE EARTH METAL FERRITES AT VARIOUS SCAN RATES

Scan rate	Specific capacitance × 10^{-3} F/g			
	$MgFe_2O_4$	$CaFe_2O_4$	$SrFe_2O_4$	$BaFe_2O_4$
0.01	63.42	99.04	288.72	130.08
0.02	42.31	56.87	186.90	79.93
0.03	35.11	43.94	135.80	60.07
0.04	32.36	36.38	121.04	45.60
0.05	31.93	30.99	93.77	37.672

Impedance (EIS) analysis was performed to know the electrochemical nature of the supercapacitor electrodes. Fig. 8 $BaFe_2O_4$, which revealed unique supercapacitor nature having a quasi-circle present in high-frequency area and a slanting line present in the low-frequency area [31,32]. The diameter estimated from the quasi-circle entails the charge-transfer resistance (R_{ct}) as electrolytic solution persuading towards the electrode [33]. $MgFe_2O_4$ (146 Ω), $SrFe_2O_4$ (155 Ω) results smaller R_{ct} (31 Ω) than $CaFe_2O_4$ (677 Ω), $BaFe_2O_4$ (751 Ω), validated huge ion migration ratio at the boundary between

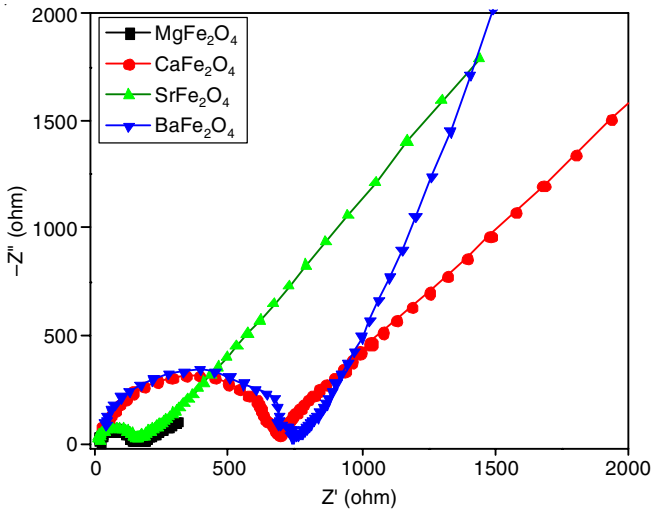

Fig. 8. Nyquist plot of synthesized alkaline earth metal ferrites

electrolytic solution and electrode [34]. All the electrodes have vertical tails present in low-frequency range, due to enhanced ionic accessibility of the electrolyte to intercalate into the internal pores.

We have extended the electrochemical studies for the prepared electrodes using graphite towards sensor applications. In this point of view, these electrodes were utilized to identify the presence of lead nitrate in 0.1 M KCl electrolyte. Fig. 9a-d

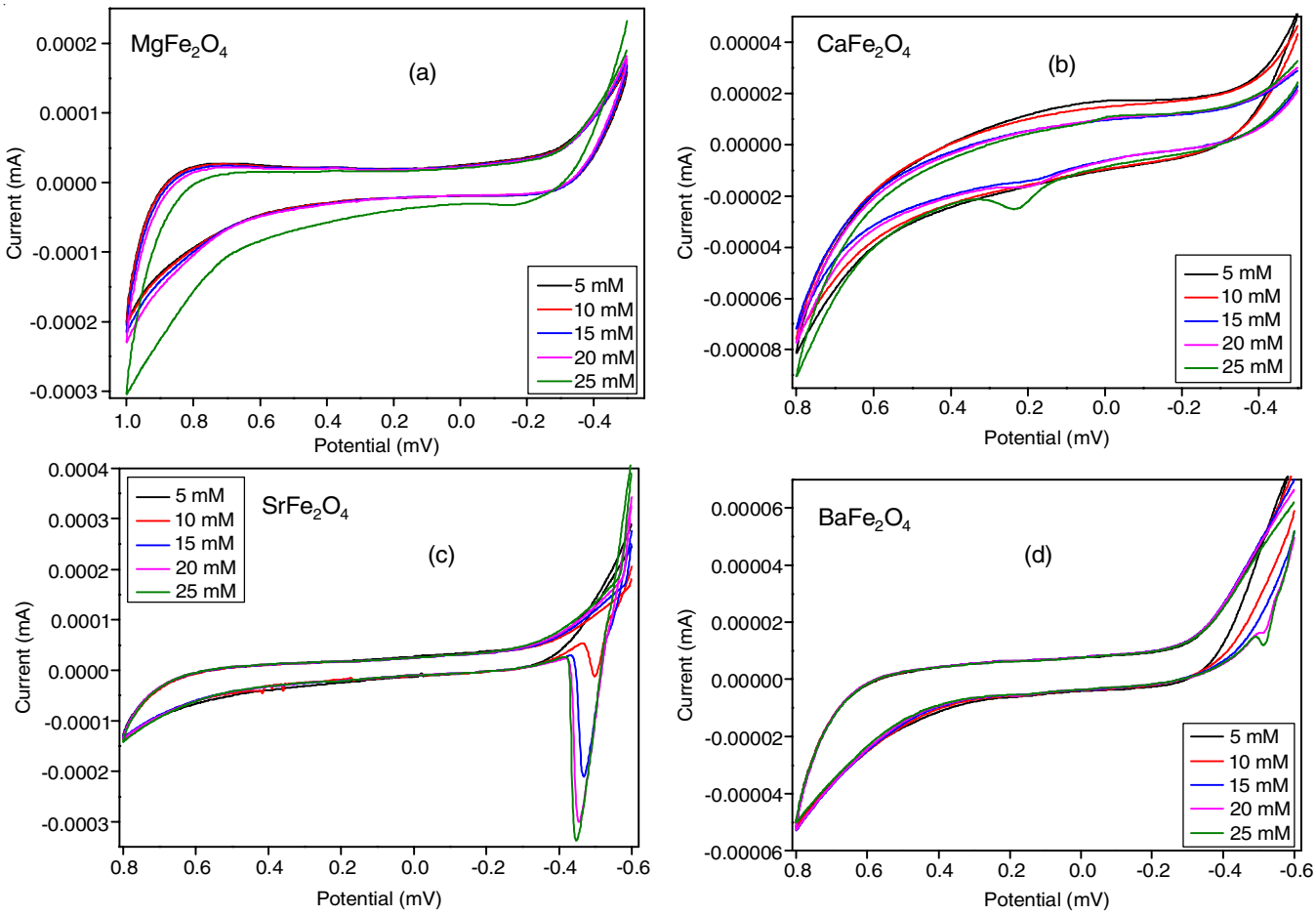

Fig. 9. Sensor study of synthesized alkaline earth metal ferrites for sensing lead nitrate

exhibit the CV curves of $MgFe_2O_4$, $CaFe_2O_4$, $SrFe_2O_4$ and $BaFe_2O_4$ electrodes for detecting lead nitrate of different concentration. As represented in Fig. 9b-d, the sensing of lead nitrate in the electrolyte was confirmed by the appearance of new reduction potential peaks as compared to the bare electrolyte. The sensibility and stability was further confirmed by increasing the concentration of lead nitrate in the electrolyte by the electrode. It was clear that $SrFe_2O_4$ detect lead nitrate at 10 mM, $CaFe_2O_4$ at 25 mM, $BaFe_2O_4$ at 20 mM, whereas $MgFe_2O_4$ didn't show any significant change compared to bare electrode. Thus, all electrodes, with the exception of $MgFe_2O_4$, are capable of functioning as a good sensor electrode in the specified electrolyte.

Conclusion

The synthesis of spinel ferrites MFe_2O_4 from alkaline earth metals (M = Mg, Ca, Sr, Ba) were performed by the solution combustion method using urea as fuel and successfully confirmed by various techniques like XRD, FTIR, SEM and UV-DRS. The resulted band gap of the ferrites was suitable for the visible light photocatalytic degradation. The enhanced degradation study for the reactive blue 4 dye solution by the ferrites might be due to its crystallinity and band gap. The $MgFe_2O_4$ results enhanced photocatalytic activity, $SrFe_2O_4$ gives better capacitance (288×10^{-3} F/g) from CV studies as well as a sensor activity towards lead nitrate at low concentration, while $CaFe_2O_4$ displays agreeable inhibition towards antibacterial activity for the bacteria *Bacillus* and *Pseudomona*s.

CONFLICT OF INTEREST

The authors declare that there is no conflict of interests regarding the publication of this article.

REFERENCES

1. A.O. Ibhadon and P. Fitzpatrick, *Catalysts*, **3**, 189 (2013); https://doi.org/10.3390/catal3010189
2. W.Y. Teoh, J.A. Scotta and R. Amal, *J. Phys. Chem. Lett.*, **3**, 629 (2012); https://doi.org/10.1021/jz3000646
3. Y. Deligiannakis, *KONA Powder Particle J.*, **35**, 14 (2018); https://doi.org/10.14356/kona.2018004
4. J.K. Patra and K.-H. Baek, **2014**, 417305 (2014); https://doi.org/10.1155/2014/417305
5. Y. Khan, H. Sadia, S.Z.A. Shah, M.N. Khan, A.A. Shah, N. Ullah, M.F. Ullah, H. Bibi, O.T. Bafakeeh, N.B. Khedher, S.M. Eldin, B.M. Fadhl and M.I. Khan, *Catalysts*, **12**, 1386 (2022); https://doi.org/10.3390/catal12111386
6. B.I. Kharisov, H.R. Dias and O.V. Kharissova, *Arab. J. Chem.*, **12**, 1234 (2019); https://doi.org/10.1016/j.arabjc.2014.10.049
7. R. Ranga, A. Kumar, P. Kumari, P. Singh, V. Madaan and K. Kumar, *Mater. Charact.*, **178**, 111269 (2021); https://doi.org/10.1016/j.matchar.2021.111269
8. M.-M. Manuel, A.-B. Deyanira, C.-M. Virginia and G.M. Jorge A, *J. Photochem. Photobiol.*, **9**, 100091 (2022); https://doi.org/10.1016/j.jpap.2021.100091

9. O. Abd-Elkader, A.M. Al-Enizi, S.F. Shaikh, M. Ubaidullah, M.O. Abdelkader and N.Y. Mostafa, *Crystals*, **12**, 393 (2022); https://doi.org/10.3390/cryst12030393
10. L. Khanna and N.K. Verma, *Mater. Sci. Semicond. Process.*, **16**, 1842 (2013); https://doi.org/10.1016/j.mssp.2013.07.016
11. P. Heidari and S.M. Masoudpanah, *J. Mater. Res. Technol.*, **9**, 4469 (2020); https://doi.org/10.1016/j.jmrt.2020.02.073
12. G.N. Rajivgandhi, G. Ramachandran, C.C. Kanisha, N.S. Alharbi, S. Kadaikunnan, J.M. Khaled, K.F. Alanzi and W.-J. Li, *Results Phys.*, **23**, 104065 (2021); https://doi.org/10.1016/j.rinp.2021.104065
13. H. Kenfoud, N. Nasrallah, O. Baaloudj, F. Derridj and M. Trari, *J. Phys. Chem. Solids*, **160**, 110315 (2022); https://doi.org/10.1016/j.jpcs.2021.110315
14. E. Casbeer, V.K. Sharma and X.Z. Li, *Sep. Purif. Technol.*, **87**, 1 (2012); https://doi.org/10.1016/j.seppur.2011.11.034
15. L. Zhang, Y. He, Y. Wu and T. Wu, *Mater. Sci. Eng. B*, **176**, 1497 (2011); https://doi.org/10.1016/j.mseb.2011.09.022
16. J.A. Jiménez-Miramontes, J.L. Domínguez-Arvizu, J.M. Salinas Gutiérrez, M.J. Meléndez-Zaragoza, A. López-Ortiz and V. Collins Martínez, *Int. J. Hydrogen Energy*, **42**, 30257 (2017); https://doi.org/10.1016/j.ijhydene.2017.09.162
17. T. Xie, L. Xu, C. Liu and X. Zhang, *Mater. Technol.*, **33**, 582 (2018); https://doi.org/10.1080/10667857.2018.1483307
18. D. Zhang and L. Zhang, *J. Taiwan Inst. Chem. Eng.*, **69**, 156 (2016); https://doi.org/10.1016/j.jtice.2016.10.015
19. R. Dom, P.H. Borse, C.R. Cho, J.S. Lee, S.M. Yu, J.H. Yoon, T.E. Hong, E.S. Jeong and H.G. Kim, *J. Ceram. Process. Res.*, **13**, 451 (2012).
20. P.H. Borse, C.R. Cho, K.T. Lim, Y.J. Lee, T.E. Hong, J.S. Bae, E.D. Jeong, H.J. Kim and H.G. Kim, *J. Korean Phys. Soc.*, **58**, 1672 (2011); https://doi.org/10.3938/jkps.58.1672
21. S. Mandizadeh, M. Salavati-Niasari and M. Sadri, *Sep. Purif. Technol.*, **175**, 399 (2017); https://doi.org/10.1016/j.seppur.2016.11.071
22. S.R. Janasi, M. Emura, F.J.G. Landgraf and D. Rodrigues, *J. Magn. Magn. Mater.*, **238**, 168 (2002); https://doi.org/10.1016/S0304-8853(01)00857-5
23. I.S. Khan and I.H. Gul, *Appl. Phys. A*, **128**, 1109 (2022); https://doi.org/10.1007/s00339-022-06214-4
24. S. Patil, K.S. Anantharaju, D. Rangappa, Y.S. Vidya, S.C. Sharma, L. Renuka and H. Nagabhushana, *Environ. Nanotechnol. Monit. Manag.*, **13**, 100268 (2020); https://doi.org/10.1016/j.enmm.2019.100268
25. N.H. Sulaiman, M.J. Ghazali, B.Y. Majlis, J. Yunas and M. Razali, *Biomed. Mater. Eng.*, **26**, S103 (2015); https://doi.org/10.3233/BME-151295
26. Y. Chen, Q. Wu, J. Wang and Y. Song, *J. Inorg. Organomet. Polym. Mater.*, **30**, 1065 (2019); https://doi.org/10.1007/s10904-019-01253-6
27. J. Singh, *Eur. J. Mol. Clin. Med.*, **7**, 3498 (2020).
28. J. Zia and U. Riaz, *J. Mater. Sci. Mater. Electron.*, **31**, 22856 (2020); https://doi.org/10.1007/s10854-020-04812-7
29. S. Meena, K.S. Anantharaju, S. Malini, A. Dey, L. Renuka, S.C. Prashantha and Y.S. Vidya, *Ceram. Int.*, **47**, 14723 (2021); https://doi.org/10.1016/j.ceramint.2020.12.217
30. O. Norouzi, S.E.M. Pourhosseini, H.R. Naderi, F. Di Maria and A. Dutta, *Sci. Rep.*, **11**, 5387 (2021); https://doi.org/10.1038/s41598-021-84979-z
31. K. Gurushantha, K.S. Anantharaju, S.C. Sharma, H.P. Nagaswarupa, S.C. Prashantha, K.R.V. Mahesh, Y.S. Vidya, H. Nagabhushana and L. Renuka, *J. Alloys Compd.*, **685**, 761 (2016); https://doi.org/10.1016/j.jallcom.2016.06.105
32. R. Liu, L. Pan, X. Liu and D. Wu, *RSC Adv.*, **5**, 16765 (2015); https://doi.org/10.1039/C4RA13720E
33. S. Meena, L. Renuka, K.S. Anantharaju, Y.S. Vidya, H.P. Nagaswarupa, S.C. Prashantha, H. Nagabhushana, *Mater. Today: Proc.*, **4**, 11773 (2017); https://doi.org/10.1016/j.matpr.2017.09.094
34. H. Wang, S. Yu and B. Xu, *Chem. Commun.*, **52**, 11512 (2016a); https://doi.org/10.1039/C6CC05911B